Three-Dimensional Thermal Structural Analysis of a Swept Cowl Leading Edge Subjected to Skewed Shock-Shock Interference Heating

Sandra P. Polesky,* Pramote Dechaumphai,† and Christopher E. Glass†
NASA Langley Research Center, Hampton, Virginia 23665
and
Ajay K. Pandey‡
Lockheed Engineering & Sciences Company, Hampton, Virginia 23665

A three-dimensional flux-based thermal analysis method has been developed and its capability is demonstrated by predicting the transient nonlinear temperature response of a swept cowl leading edge subjected to intense three-dimensional aerodynamic heating. The predicted temperature response from the transient thermal analysis is used in a linear elastic structural analysis to determine thermal stresses. Predicted thermal stresses are compared with those obtained from a two-dimensional analysis which represents conditions along the chord where maximum heating occurs. Results indicate that a three-dimensional analysis could be required to predict accurately the leading edge thermal stress response.

Nomenclature

c	=	specific heat
E, F, G	=	x, y, and z flux components, respectively
H	=	heat load
h	=	convective heat transfer coefficient
k	=	thermal conductivity
ℓ	=	chordwise coordinate
M	=	Mach number
[M]	=	mass matrix
{N}	=	vector of element interpolation functions
[N]	=	row matrix of element interpolation functions
q	=	aerodynamic heating
q_x, q_y, q_z	=	components of heat flux in x, y, and z coordinate directions, respectively
$\{R\}$	=	load vector
r	=	radius
S	=	spanwise coordinate
T	=	temperature
T_r	=	fluid recovery temperature
T_∞	=	surrounding medium temperature
t	=	time
U	=	conservation variable
V	=	element volume
x, y, z	=	coordinate directions
Λ	=	sweep angle
ΔT	=	change in temperature per time step
Δt	=	time step
ΔU	=	change in conservation variable per time step
ε	=	emissivity
θ	=	circumferential angle
σ	=	Stefan-Boltzmann constant
σ_C	=	normal stress in chordwise direction
σ_S	=	normal stress in spanwise direction
$\sigma_x, \sigma_y, \sigma_z, \tau_{xy}, \tau_{xz}, \tau_{yz}$	=	components of stress tensor

Subscripts

S	=	structural
T	=	thermal
1	=	element internal flux
2	=	flux across element boundary

Superscripts

n	=	time step index, $t^n = n\Delta t$
T	=	transpose

Introduction

THE ability to predict accurately the structural response induced by thermal effects is an important factor in the structural design of high-speed aerospace vehicles. Intense aerodynamic heating of hypersonic vehicles which operate at high Mach numbers may produce severe thermal stresses that can reduce the structural performance and may cause structural failure. Detailed temperature distributions are required for the structural analysis to predict the thermal stresses accurately. Research is underway at NASA Langley Research Center to develop efficient computational methods to predict accurately the thermal-structural response of hypersonic aircraft subjected to severe thermal loading conditions.

A two-dimensional, flux-based, finite element method has been used recently to predict the aerodynamic flow-field and thermal-structural response for high-speed flow over leading edges.[1] This integrated approach applies a Taylor-Galerkin algorithm to the governing equations expressed in conservation form. The flux-based finite element method has computational benefits over conventional, nonlinear finite element analysis capabilities.[2] For example, this formulation results in finite element matrices that can be evaluated in closed form, thereby, avoiding the expensive numerical integration which is required in conventional finite element codes. Also, ma-

Presented as Paper 90-1710 at the AIAA/ASME Fifth Thermophysics and Heat Transfer Conference, Seattle, WA, June 18–20, 1990; received June 15, 1990; revision received and accepted for publication Nov. 26, 1990.

*Aerospace Technologist, Aircraft Structures Branch.
†Aerospace Technologist, Aerothermal Loads Branch. Member AIAA.
‡Principal Engineer. Member AIAA.

terial nonlinearities can be implemented easily without requiring regeneration of the finite element matrices. Because these advantages improve computational efficiency over conventional methods, the flux-based algorithm should be more suitable for solving complex problems.

During hypersonic flight, the flow field over a leading edge is normally three dimensional, therefore, the leading edge requires a fully three-dimensional thermal-structural analysis. To accommodate this need, the flux-based algorithm of reference 1 has been extended to include a three-dimensional, linear, quasi-static structural analysis capability.[2] In this paper, the flux-based algorithm is further extended to include a three-dimensional, nonlinear thermal analysis capability. The focus of the paper is the application and evaluation of this three-dimensional analysis capability to predict the thermal-structural response of an actively cooled swept-cowl leading edge subjected to skewed shock-shock interference heating. Mechanical loads, such as the external aerodynamic pressure and the internal coolant pressure, are neglected in the analysis. Results are compared to those obtained from a two-dimensional analysis of the leading edge.

Thermal-Structural Formulation

Governing Equations

Heat Transfer

The transient thermal response of the structure is governed by the energy equation, which, in conservation form, can be written as

$$\frac{\partial U_T}{\partial t} + \frac{\partial (E_T)}{\partial x} + \frac{\partial (F_T)}{\partial y} + \frac{\partial (G_T)}{\partial z} = H_T \tag{1}$$

where the subscript T denotes the thermal formulation, U_T is the conservation variable, E_T, F_T, and G_T are the heat flux components, and H_T is the heat source term. For transient heat conduction with no internal heat source, these quantities are

$$\partial U_T = \rho c \partial T; \quad E_T = q_x = -k\frac{\partial T}{\partial x}; \quad F_T = q_y$$

$$= -k\frac{\partial T}{\partial y}; \quad G_T = q_z = -k\frac{\partial T}{\partial z}; \quad H_T = 0 \tag{2}$$

where ρ is the density, c is the specific heat, k is the thermal conductivity, and T is the temperature. As shown in Eq. (2), the components of heat flux in the three coordinate directions (q_x, q_y, and q_z) are assumed to be related to temperature gradients by Fourier's law. Both specific heat and thermal conductivity may be temperature dependent.

Structural Response

The formulation of the structural equations is covered in detail in Ref. 2, and only the governing equation is given here to show the generality of the flux-based algorithm. The static structural response is governed by the equilibrium equations in conservation form

$$\frac{\partial \{E_S\}}{\partial x} + \frac{\partial \{F_S\}}{\partial y} + \frac{\partial \{G_S\}}{\partial z} = 0 \tag{3}$$

where the subscript S denotes the structural formulation. The vectors $\{E_S\}$, $\{F_S\}$, and $\{G_S\}$, which contain the stress components are given by

$$\{E_S\}^T = [\sigma_x \quad \tau_{xy} \quad \tau_{xz}]$$

$$\{F_S\}^T = [\tau_{xy} \quad \sigma_y \quad \tau_{yz}]$$

$$\{G_S\}^T = [\tau_{xz} \quad \tau_{yz} \quad \sigma_z] \tag{4}$$

where the stress components σ_x, σ_y, σ_z, τ_{xy}, τ_{xz}, and τ_{yz} are assumed to be related to displacement gradients and the temperature by generalized Hooke's law.

Solution Procedure

For simplicity, the thermal or structural conservation equation is written in the form of a single equation as

$$\frac{\partial U}{\partial t} + \frac{\partial E}{\partial x} + \frac{\partial F}{\partial y} + \frac{\partial G}{\partial z} = 0 \tag{5}$$

where the first term is zero for the quasi-static structural formulation.

An explicit, first-order-accurate, time-marching algorithm, the flux-based Taylor-Galerkin algorithm, is used to solve the energy equation for the temperature distribution at various time steps. The basic concepts of the Taylor-Galerkin algorithm are to 1) use a Taylor series expansion of the conservation variable in time to establish recurrence relations for time marching, 2) eliminate the time derivatives in the Taylor series using the governing equation, and 3) use the Galerkin method of weighted residuals[3] for spatial discretization. A detailed description of the Taylor-Galerkin algorithm is given in Refs. 4 and 5.

The structural equilibrium equations are also discretized using the Galerkin method of weighted residuals. The structural formulation is quasi-static in that the discretized equilibrium equations are solved using the temperature solution from a particular time level as the structural load. The feature of the flux-based algorithm, which differs from the conventional finite element method, is to express the variation of the element fluxes E, F, and G in the same form as the element dependent variable U, that is

$$\begin{aligned} U(x,y,z,t) &= [N(x,y,z)]\{U(t)\} \\ E(x,y,z,t) &= [N(x,y,z)]\{E(t)\} \\ F(x,y,z,t) &= [N(x,y,z)]\{F(t)\} \\ G(x,y,z,t) &= [N(x,y,z)]\{G(t)\} \end{aligned} \tag{6}$$

where $[N(x,y,z)]$ is the row matrix which contains the element interpolation functions for an 8-noded hexahedral element, and $\{E\}$, $\{F\}$, and $\{G\}$ are the vectors of the element nodal quantities. This feature removes the necessity of reforming the element matrices at every time step when temperature dependent material properties are modeled.

Finite Element Equations

The transient thermal finite element equation is written in the form

$$[M]\{\Delta U\}^n = \{R\}_1^n + \{R\}_2^n \tag{7}$$

where $[M]$ denotes the mass matrix

$$[M] = \int_v \{N\}[N]\mathrm{d}V \tag{8}$$

which is diagonalized by correcting the mass at the node points. The vectors $\{R\}_1$ and $\{R\}_2$ are associated with the fluxes within the element and across the element boundary, respectively, and $\{\Delta U\}^n$ is the change in the conservation variable between the time steps t^{n+1} and t^n where $t^n = n\Delta t$. These vectors are defined by

$$\{R\}_1 = \Delta t \left(\int_v \frac{\partial \{N\}}{\partial x}[N]\mathrm{d}V\{E\} + \int_v \frac{\partial \{N\}}{\partial y}[N]\mathrm{d}V\{F\} + \int_v \frac{\partial \{N\}}{\partial z}[N]\mathrm{d}V\{G\} \right) \tag{9}$$

$$\{R\}_2 = -\Delta t \int_s \{N\}[N]\mathrm{d}S\{q\} \qquad (10)$$

The vector $\{q\}$ contains the components of the nodal heat flux normal to the element surface boundary. The thermal boundary conditions are applied via the vector $\{q\}$ expressed in Eq. (10), where the surface nodal heat flux q is replaced by the quantities representing any one of several different types of boundary conditions

$$q = \begin{cases} 0 & \text{(insulated)} \\ q_S & \text{(specified heating)} \\ h(T - T_r) & \text{(surface convection)} \\ \varepsilon\sigma(T^4 - T_\infty^4) & \text{(surface radiation)} \end{cases} \qquad (11)$$

The structural analysis, which uses the linear flux formulation, produces matrices identical to Eqs. (9) and (10), where E, F, and G are replaced by the nodal stress components given in Eq. (4). More details on the formulation and boundary conditions for the structural analysis are described in Ref. 2.

In the present three-dimensional, finite-element, flux-based thermal analysis code, $\{N(x,y,z)\}$ contains the element interpolation functions for 8-noded, solid hexahedral elements. The finite element equation, Eq. (7), is solved for the change in the conservation variable by explicit time marching. The change in the temperatures are then obtained from the change in the conservation variable at each time step, where $\Delta U = \rho c \Delta T$. The nodal heat fluxes are then evaluated—for example, in the x direction, by assuming that $\partial T/\partial x = (\partial[N]/\partial x)\{T\}$—using the updated temperatures.

For the flux-based formulation, all element integrals, which are given in Eqs. (8)–(10), can be evaluated in closed form. The use of these closed form expressions for the 8-noded hexahedral element has been shown to reduce the computation time in the structural analysis code by a factor of five compared to conventional finite element codes using numerical integration.[2] Also, since the conductivity term is included in the heat flux vectors in Eq. (9), regeneration of the element matrices is not required for temperature dependent thermal conductivity.

Application

A hypersonic vehicle concept, its scramjet engine inlet, and the flow pattern surrounding a cowl leading edge segment are shown schematically in Fig. 1. The cowl leading edge consists of a series of leading edge segments that are swept back 45 deg and arranged in a sawtooth pattern as shown in the figure. In hypersonic flight, the vehicle nose bow shock must be located close to the engine cowl bow shock if maximum mass capture at the engine inlet and efficient engine performance is to be achieved. A change in vehicle flight conditions can cause the vehicle nose bow shock to pass across the engine cowl bow shock producing a skewed shock-shock interaction flow pattern surrounding the swept cowl leading edge. For a Mach 16 flight condition, the portion of the cowl leading edge above the vehicle nose bow shock is exposed to Mach 10 flow which is turned 7 deg downward by the vehicle underbody as shown in Fig. 2. The vehicle nose bow shock is at a 10 deg incline as it intersects the 45 deg swept cowl leading edge, which causes the shock-shock interaction to be skewed along the span of the leading edge.

Several types of interference patterns[6,7] will be present along the span of the swept cowl leading edge due to the skewed shock-shock interaction. At the span location $S = 0$, where the vehicle nose bow shock intersects the upper portion of the cowl bow shock, a shock/boundary-layer interference pattern is present. The interference pattern changes along the span due to the skewed orientation of the shock-shock interaction. At the span location where the vehicle nose bow shock intersects perpendicular to the cowl bow shock, a supersonic

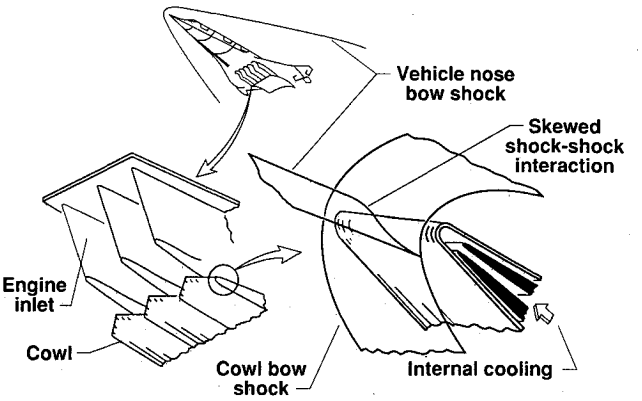

Fig. 1 Aerospace plane, scramjet engine inlet, and flow interaction for engine cowl leading edge.

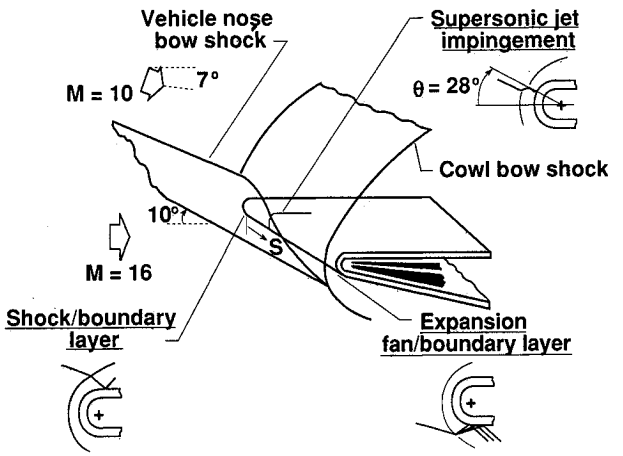

Fig. 2 Skewed shock-shock interference patterns along span of cowl leading edge.

jet impingement occurs. This interference pattern results in a significant amplification of the heating rate on the leading edge surface and is referred to as a Type IV interference condition.[7] An expansion-fan/boundary-layer interference pattern occurs at the other end of the span, where the vehicle nose bow shock intersects the lower portion of the cowl bow shock. The heat load on the surface of the cowl leading edge produced by this skewed shock-shock interference pattern is used to determine the thermal-structural response of the cowl leading edge for this study.

Aerodynamic Heating

The aerodynamic heating rates on the surface of the swept cowl leading edge used in the present thermal-structural analysis are based on results from an experimental study of a swept cylindrical leading edge subjected to shock wave interference.[8] The experimental setup produced quasi-two-dimensional shock interference patterns, which were used to approximate a three-dimensional heating distribution for the present configuration and freestream conditions as follows: The heating rate distributions on the leading edge surface due to the assumed interference patterns were chosen to match the shapes of those obtained experimentally. The maximum heating rate for a Mach 16 flight conditon and a leading-edge radius of 0.125 in. was calculated for a zero sweep angle by the EASI code[9] and then corrected to account for a sweep angle of 45 deg.[8] The corrected maximum heating level was then imposed on the experimental heating distributions. The resulting heating rate distributions for the various interference patterns were linearly interpolated to form a three-dimensional surface heating distribution along the span of the cowl leading edge. The resulting aerodynamic heating rate distri-

bution on the upper surface of the cowl leading edge is shown schematically in Fig. 3. Intense localized heating with a maximum value of 29,700 Btu/ft²-s occurs at a region on the surface of the leading edge where the supersonic jet impinges on the swept leading edge. The location of maximum heating is about 28 deg above the stagnation line on the cowl leading edge.[8]

Previous two-dimensional analyses using a transient heat load for the condition where the nose bow shock sweeps across the cowl bow shock have shown that almost the same results would be obtained if the problem were solved quasi-statically.[1] Therefore, a steady aerodynamic heat load was used in the present analysis.

Finite Element Models

The three-dimensional finite element model, used in both the thermal and structural analysis, utilizes 8-noded hexahedral elements which is shown in Fig. 4. The model consists of 3696 nodes, 43 elements chordwise, 13 elements spanwise, and 5 elements through the thickness. The leading edge model has an outer radius of 0.125 in., an inner radius of 0.110 in., a chord length of 3 in. at $z = 0$, and a span width of 1.5 in. at the nose portion of the leading edge. As shown in the figure, the model is swept back 45 deg with respect to the z-coordinate direction at $y = 0$, and the upper surface of the model is parallel to the y coordinate direction where the lower surface is at a 6 deg incline with respect to the y coordinate direction. This finite element model is an idealization of the cowl leading edge skin and neglects any connection with the inner structure of the leading edge.

The leading edge material is assumed to be copper because its high thermal conductivity enables the reduction of the leading edge temperatures and temperature gradients by diffusion of the heat. The temperature-dependent material properties for copper[10] used in the transient thermal analysis are shown in Fig. 5. All of the model boundary conditions used

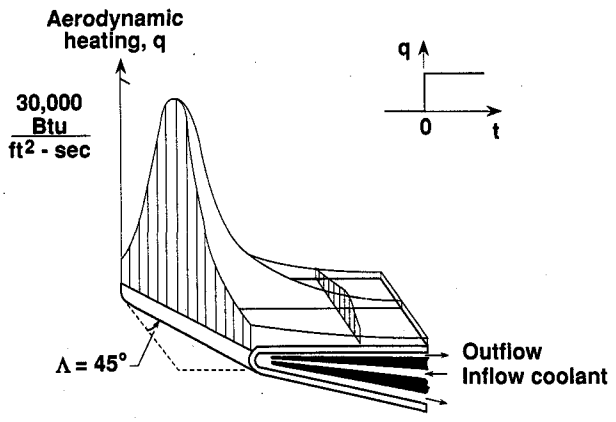

Fig. 3 Three-dimensional aerodynamic heating distribution on surface of swept cowl leading edge.

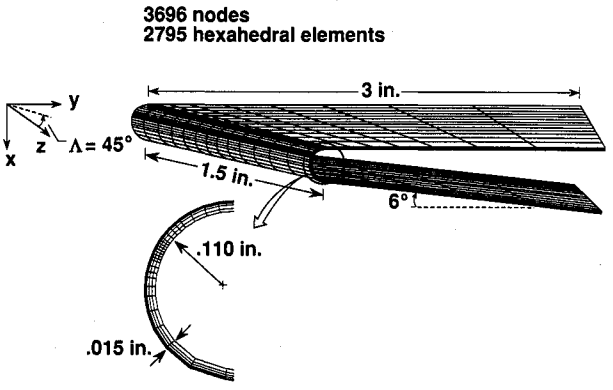

Fig. 4 Thermal and structural finite element model.

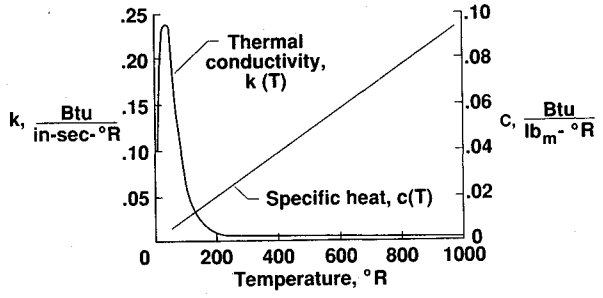

Fig. 5 Temperature dependent properties for copper.

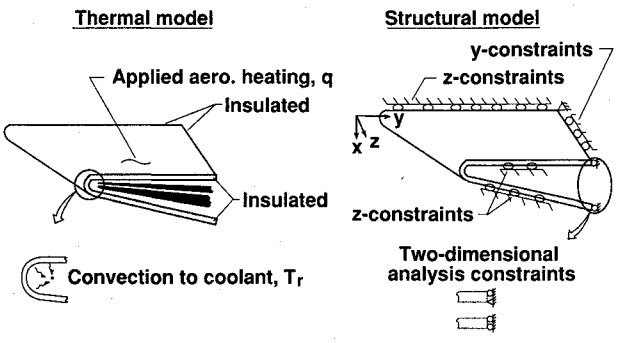

(a) Thermal analysis **(b) Structural analysis**

Fig. 6 Boundary conditions

in the thermal analysis are shown in Fig. 6a. The aerodynamic heating distribution, described previously and shown schematically in Fig. 3, is applied to the outer surface. The inner surface is convectively cooled with an assumed constant convection heat transfer coefficient of 7.85 Btu/ft²-s-R, a value achievable locally by the impingement of a sonic hydrogen jet. In addition, this convection heat transfer coefficient was doubled in the thermal analysis to represent the increased cooling effectiveness of fins which would be present on the inner surface of the leading edge skin if the geometry were modeled in more detail. The initial temperature throughout the model is equivalent to the coolant temperature of 50° R and the inner surface convects heat to the coolant which is assumed to be at a constant temperature of 50° R.

For the structural analysis, the leading edge model was subjected to thermal loading only, using the steady-state temperature distribution obtained from the thermal analysis and a reference temperature of 530° R for the zero stress state. Two sets of boundary conditions were studied in analyzing the structural response of the leading edge model. The first set of boundary conditions, for the case where both ends of the span were fixed, are shown in Fig. 6b. The z constraints shown in the figure prevent the nodes at both ends of the span from moving in the z direction and the y constraints prevent the nodes from moving in the y direction. The pin constraint shown in the figure prevents motion in all directions. The second set of boundary conditions studied were for a free end condition where the z constraints at the end of the span, where $z = 1.5 \cos 45$ deg in., were removed from the model.

The two-dimensional thermal-structural model used for comparisons in the present study was obtained by taking a two-dimensional slice of the three-dimensional model in the chordwise direction. The location of this slice is the span location where the supersonic jet impingement occurs and the heating is a maximum. The two-dimensional model contains one layer of hexahedral elements in the z direction and the same element discretization in the x–y plane as the three-dimensional model shown in the detailed enlargement of the leading edge nose in Fig. 4. For the two-dimensional plane strain structural analysis, where the structural boundary conditions are shown in Fig. 6b, the leading edge model is sub-

jected to thermal loading obtained from a two-dimensional thermal analysis. Results of the transient thermal and quasi-static structural analyses are presented in the following section.

Results and Discussion

Thermal Analysis

Calculated temperature histories at four different locations on the surface of the leading edge, labeled Points A through D, are shown in Fig. 7. The high thermal diffusivity of the .015-in. thick copper leading edge results in a rapid thermal response of the structure, and the solution reaches a steady-state condition in approximately 0.02 sec. Point B is the location where the maximum heating rate occurs on the surface of the leading edge as a result of the supersonic jet impingement. At Point B, a maximum temperature of 1000° R is achieved for the steady-state condition. Points A, C, and D were arbitrarily selected to show the large difference in the steady-state temperature solution at points located farther away from the supersonic jet impingement location. The circumferential surface heating rate distribution on the leading edge nose at the span location where the supersonic jet impingement occurs is shown in Fig. 8. The curve describes the surface heating rate, q, as a function of the angular location, θ, along the circumference of the leading edge nose. A maximum heating rate of 27,900 Btu/ft^2-s occurs at θ = 28 deg, the location where the supersonic jet impingement occurs. The finite element nodes of the discretized leading edge were

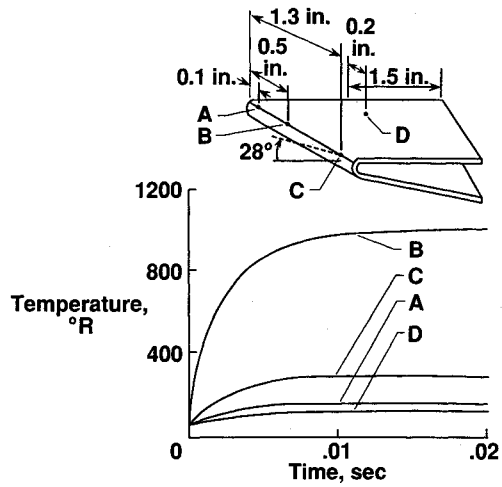

Fig. 7 Transient surface temperatures at several point locations on surface of leading edge.

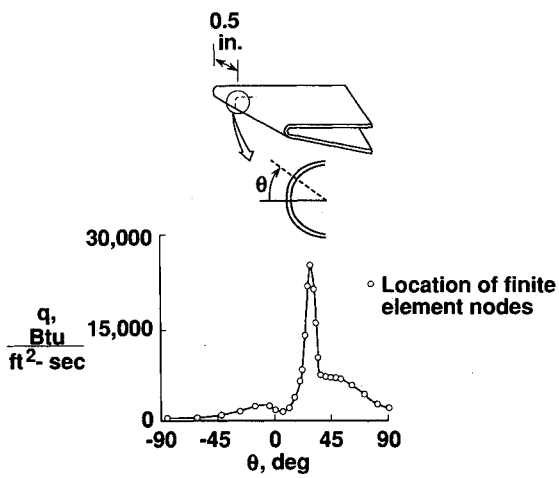

Fig. 8 Circumferential surface heating rate distribution on leading edge nose at span location, S = 0.5 in.

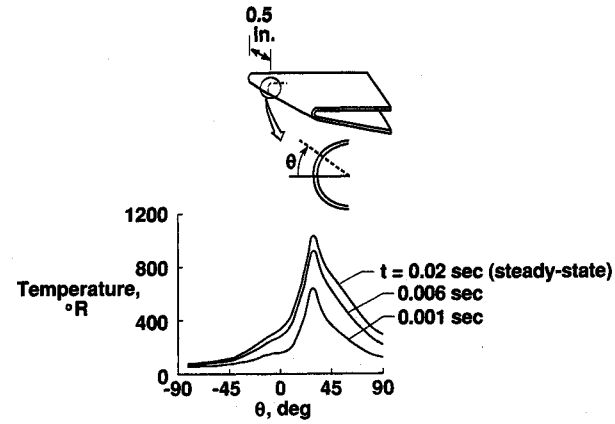

Fig. 9 Circumferential surface temperature distributions at S = 0.5 in., for three times during transient thermal analysis.

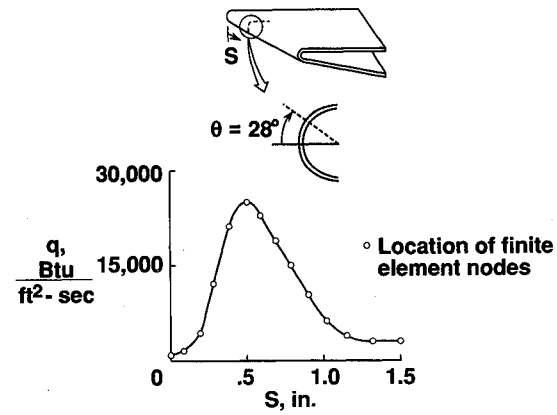

Fig. 10 Spanwise surface heating rate distribution at θ = 28 deg.

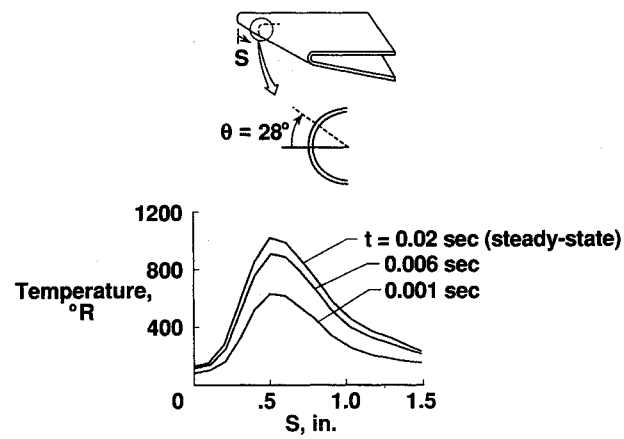

Fig. 11 Spanwise temperature distribution at θ = 28 deg, for three times during transient thermal analysis.

located to represent the thermal gradients based on this heating rate distribution and are shown by the symbols in the figure. Corresponding transient surface temperature distributions are shown in Fig. 9 for three values of time of the transient thermal response. This figure reveals a peak temperature of 1000° R at θ = 28 deg for the curve at t = 0.02 sec, which has been shown to be the steady-state condition in Fig. 7. Although this figure indicates large temperature gradients at all three times shown, the maximum temperature gradient, 19,804° R per in. at θ = 25 deg, occurs for the steady-state condition. Since thermal stress is dependent on thermal gradients, the steady-state temperatures are a likely candidate for use as the thermal loading in the structural analysis for determining maximum thermal stress. The spanwise surface heating rate distribution of θ = 28 deg is shown

in Fig. 10. This curve represents the heating rate, q, as a function of location along the leading edge span, S, at the circumferential location $\theta = 28$ deg on the leading edge nose. The leading edge model was discretized in the spanwise direction based on this heating rate distribution, where the node locations are shown by the symbols. The corresponding spanwise surface temperature distributions along $\theta = 28$ deg are shown in Fig. 11 for three values of time during the transient thermal analysis. As with the circumferential temperature gradients, the maximum spanwise temperature gradient occurs for $t = 0.02$ sec, the steady-state condition, although the curves for lower values of time also show large temperature gradients. A relatively large spanwise temperature gradient of 3052° R per in. between s = 0.3 and s = 0.4 in. occurs for the steady-state condition due to the skewed orientation of the incident shock. Transient temperature distributions through the thickness of the leading edge at the supersonic jet impingement location are shown for three values of time in Fig. 12. Also shown is a contour plot of the temperature distribution along a chordwise slice for the steady-state condition. The nearly linear temperature distributions through the thickness of the leading edge for the three times shown confirms the ability of copper to diffuse heat rapidly through the thickness. Because the inner surface of the leading edge is subjected to convection cooling with a coolant temperature of 50° R, a maximum temperature gradient of 26,000° R per inch through the thickness occurs near the outer surface for the steady-state condition. The high density of contour lines at the nose of the leading edge indicates that large temperature gradients exist through the thickness of the leading edge at the location of the supersonic jet impingement.

A contour plot of the steady-state surface temperatures is shown in Fig. 13. A peak temperature of 1000° R occurs at the location where the supersonic jet impinges on the surface. The high density of contour lines in the vicinity of the peak are associated with large temperature gradients on the surface of the leading edge. The temperature distributions presented and shown in Figs. 9, 11, and 12 reveal maximum temperature gradients for the steady-state condition at $t = 0.02$ sec. Therefore, the steady-state temperature response for the leading edge is used for the thermal loading in the static structural analysis to determine the maximum thermal stresses.

Structural Analysis

A contour plot of the normal thermal stresses in the spanwise directions (σ_S) on the surface of the leading edge model is shown in Fig. 14 for the case where both ends of the span are fixed. A maximum compressive stress of −300 ksi is observed near the location of the supersonic jet impingement. Since the yield stress for copper is only 25–30 ksi, these results suggest that a plastic analysis is necessary to predict realistic thermal stresses for this case. A contour plot of the normal thermal stresses in the spanwise direction (σ_S) on the surface of the leading edge model for the case where one end of the span is free to move is shown in Fig. 15. A maximum compressive stress of −300 ksi is predicted, which once again would indicate a need for a plastic analysis. A point of interest is both cases predicted the same maximum compressive stress of −300 ksi. Having the same maximum thermal stress for the free-end case as for the fixed-end case indicates that the peak stress is due to the local thermal gradients and the effect of boundary conditions is negligible. The thermal displacements obtained for the free-end case results in the leading edge deformation shape shown in Fig. 16. This figure indicates large deformations in the vicinity of the supersonic jet impingement compared to the rest of the leading edge model.

Thermal stress results from the two-dimensional, plane strain structural analysis are compared in Figs. 17 and 18 with the three-dimensional results, for both the fixed-end and free-end boundary condition cases. The normal stresses in the spanwise direction are plotted as a function of the chordwise coordinate, ℓ, at the span location of the supersonic jet impingement

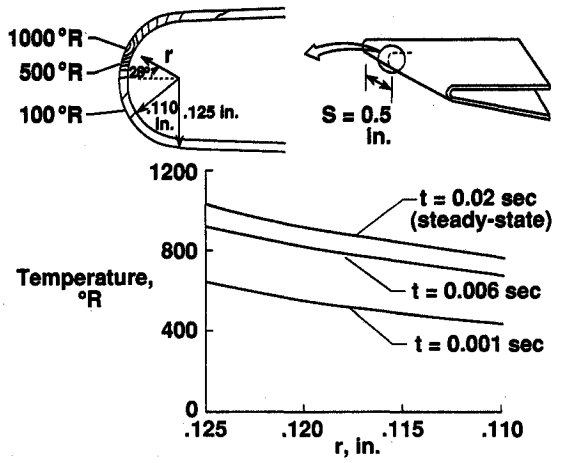

Fig. 12 Steady-state temperature contours at $S = 0.5$ in., and transient temperature distributions through thickness of leading edge at $S = 0.5$ in. and $\theta = 28$ deg, for three times during transient thermal analysis.

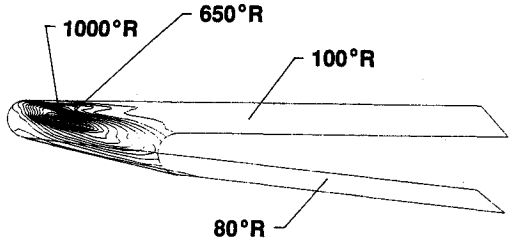

Fig. 13 Steady-state temperature contours on leading edge surface.

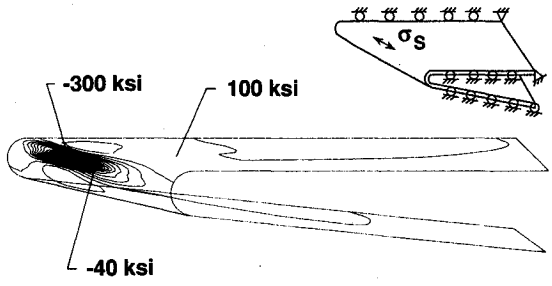

Fig. 14 Spanwise stress contours for both ends fixed boundary conditions.

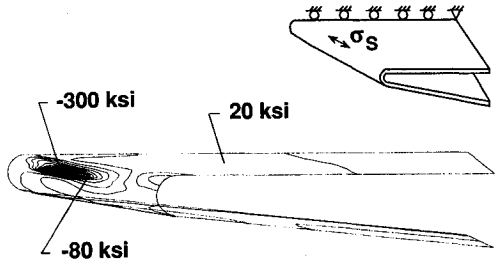

Fig. 15 Spanwise stress contours for one end fixed and one end free-boundary conditions.

as shown in Fig. 17. All three cases show relatively low stresses over most of the chord with a large spike occurring in the region where the supersonic jet impinges on the surface. The maximum spanwise stress predicted from the two-dimensional plane strain analysis (−380 ksi) is 26% greater than that predicted from the three-dimensional analysis (−300 ksi). Since the temperature distribution obtained from the two-dimensional thermal analysis was found to be nearly the same as that obtained from the three-dimensional analysis at this span location, the difference is due to the spanwise temper-

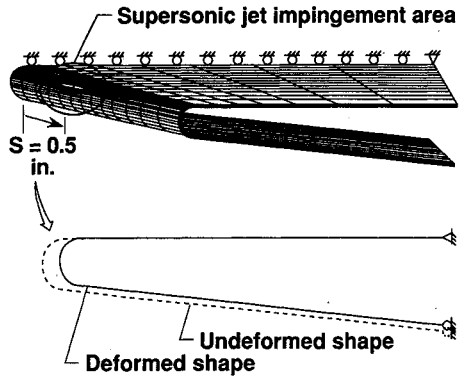

Fig. 16 Leading edge deformation shape for free end boundary conditions.

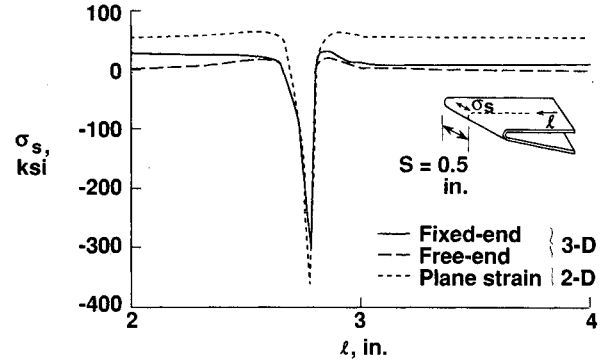

Fig. 17 Chordwise variation of spanwise normal stress at span location, S = 0.5 in.

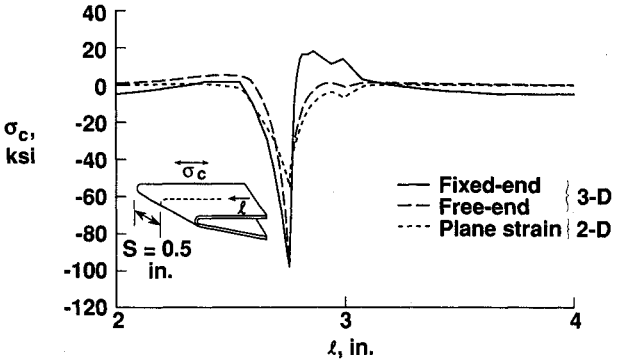

Fig. 18 Chordwise variation of chordwise normal stress at span location, S = 0.5 in.

ature gradients. The normal chordwise stresses are plotted as a function of the chordwise coordinate at the span location of the supersonic jet impingement in Fig. 18. The chordwise stress distribution shape resembles the spanwise stress distribution, but the magnitude of the chordwise stresses are much less than the spanwise stresses. However, the maximum chordwise stress predicted from the two-dimensional plane strain analysis (−60 ksi) is 40% below the maximum chordwise stress of −100 ksi predicted from the three-dimensional analyses.

Concluding Remarks

A flux-based finite element formulation was developed and used to predict the three-dimensional thermal-structural response of a swept cowl leading edge subjected to skewed shock-shock interference heating. The thermal analysis revealed large temperature gradients for the swept cowl leading edge due to the intense, localized point heating caused by the impingement of a supersonic jet and the skewed orientation of the incident shock from the vehicle nose. Since maximum temperatures and thermal gradients occurred during the steady-state condition, these temperatures were used in the structural analysis to calculate thermal stresses. A maximum compressive stress of −300 ksi was predicted for both the fixed-end and free-end boundary condition cases studied. Therefore, boundary condition effects were negligible because the localized maximum stress was due to large thermal gradients in the vicinity of the supersonic jet impingement, and the distance from this region to the boundaries was relatively large. Since the yield stress for copper is only 25–30 ksi, the results suggest that a plastic analysis is needed to determine realistic thermal stresses and the resulting deformations for the leading edge model. Finally, results from the three-dimensional structural analysis may differ substantially from those of two-dimensional analyses—as much as 40% in the present case. Because the two-dimensional analysis was shown in this study to be unconservative by predicting lower chordwise stresses, it is concluded that three-dimensional analyses could be required in future evaluations of leading edge designs.

References

[1]Dechaumphai, P., Thornton, E. A., and Wieting, A. R., "Flow-Thermal-Structural Study of Aerodynamically Heated Leading Edges," *AIAA Journal of Spacecraft and Rockets*, Vol. 26, No. 4, 1989, pp. 201–209.

[2]Pandey, A. K., and Dechaumphai, P., "Thermal-Structural Finite Element Analysis Using Linear Flux Formulation," AIAA Paper 89-1224-CP, April 1989.

[3]Huebner, K. H., and Thornton, E. A., *The Finite Element Method for Engineers*, Wiley, New York, 1982.

[4]Thornton, E. A., and Dechaumphai, P., "Coupled Flow, Thermal and Structural Analysis of Aerodynamically Heated Panels," *Journal of Aircraft*, Vol. 25, Nov. 1988, pp. 1052–1059.

[5]Thornton, E. A., and Dechaumphai, P., "Finite Element Prediction of Aerothermal-Structural Interaction of Aerodynamically Heated Panels," American Institute of Aeronautics and Astronautics 22nd Thermophysics Conference, AIAA Paper 87-1610. Honolulu, Hawaii, June 8–10, 1987.

[6]Wieting, A. R., "Experimental Study of Shock Wave Interference Heating on a Cylindrical Leading Edge," NASA TM-100484, May 1987.

[7]Edney, Barry: "Anomalous Heat Transfer and Pressure Distributions on Blunt Bodies at Hypersonic Speeds in the Presence of a Impinging Shock," The Aeronautical Research Institute of Sweden, FFA Report 115, Feb. 1968.

[8]Glass, Christopher E., "Experimental Study of Pressure and Heating Rate on a Swept Cylindrical Leading Edge From Shock wave Interference," M. S. Thesis, Old Dominion University, Norfolk, Virginia, April 1989.

[9]Glass, Christopher E., "Computer Program Which Solves Two-Dimensional /Shock Wave Interference Problems Using An Equilibrium Chemically Reacting Air Model," NASA TM-4187, 1990.

[10]Touloukian, Y. S., Powell, R. W., Ho, C. Y., and Klemens, P. G., "Thermal Conductivity for Metallic Elements and Alloys," *Thermophysical Properties of Matter*, Vol. 1, IFI/Plenum, New York, 1970.